

Improving subtropical boundary layer cloudiness in the 2011 NCEP GFS

Jennifer K Fletcher¹, Christopher S Bretherton², Heng Xiao³, Ruiyu Sun⁴, and Jongil Han⁵

¹Monash University, Clayton, Victoria, Australia

²University of Washington, Seattle, Washington, United States

³Pacific Northwest National Laboratory, Richland, Washington, United States

⁴IMSG at NOAA/NWS/NCEP/EMC, Camp Springs, Maryland, United States

⁵SRG at NOAA/NWS/NCEP/EMC, Camp Springs, Maryland, United States

Correspondence to: Jennifer K Fletcher
(jennifer.fletcher@monash.edu)

Abstract. The current operational version of National Centers for Environmental Prediction (NCEP) Global Forecasting System (GFS) shows significant low cloud bias. These biases also appear in the Coupled Forecast System (CFS), which is developed from the GFS. These low cloud biases degrade seasonal and longer climate forecasts, particularly of shortwave cloud radiative forcing, and affect predicted sea-surface temperature. Reducing this bias in the GFS will aid the development of future CFS versions and contributes to NCEP's goal of unified weather and climate modelling.

Changes are made to the shallow convection and planetary boundary layer parametrisations to make them more consistent with current knowledge of these processes and to reduce the low cloud bias. These changes are tested in a single-column version of GFS and in global simulations with GFS coupled to a dynamical ocean model. In the single column model, we focus on changing parameters that set the following: the strength of shallow cumulus lateral entrainment, the conversion of updraught liquid water to precipitation and grid-scale condensate, shallow cumulus cloud top, and the effect of shallow convection in stratocumulus environments. Results show that these changes improve the single-column simulations when compared to large eddy simulations, in particular through decreasing the precipitation efficiency of boundary layer clouds. These changes, combined with a few other model improvements, also reduce boundary layer cloud and albedo biases in global coupled simulations.

1 Introduction

The National Centers for Environmental Prediction (NCEP) Global Forecast System (GFS, <http://www.emc.ncep.noaa.gov/GFS/doc.php>) is an important model for operational weather forecasting. A frozen version of the GFS is coupled to the Modular Ocean Model v4 (<http://www.gfdl.noaa.gov/mom-ocean-model>) and called the Coupled Forecast System (CFS); this is used for seasonal to inter-decadal climate predictions and reanalyses (Saha et al., 2006, 2010). An outstanding problem for both the GFS and CFS, described in more detail below, is the representation of boundary layer clouds. We focus on improving parametrisation of these clouds and their associated processes in the GFS, using insights gained from parametrisation development work in climate models and studies using large eddy simulation.

This research was conducted collaboratively by researchers at the University of Washington and NCEP, funded as part of a NOAA-funded Climate Process Team (CPT) on the Stratocumulus-Cumulus Transition. The purpose of the CPT was to improve the representation of subtropical boundary-layer cloud processes in the GFS and CFS, as well as in the Community Earth System Model (CESM, <http://www.cesm.ucar.edu/>), using the relative strengths and weaknesses of these two rather different modelling systems to help inform further parametrisation advances in both models. The CPT has also involved researchers from the Jet Propulsion Laboratory, University of California Los Angeles, the National Center for Atmospheric Research (NCAR), and Lawrence Livermore National Laboratories.

It is anticipated that Version 3 of the CFS will be developed from an upcoming operational version of the GFS, making current biases in the GFS relevant to forecasts of seasonal and longer timescales. Xiao et al. (2014) presented our CPT's comparisons of the simulated climate from multidecadal free-running simulations using an ocean-coupled version of the GFS operational in late 2011 with comparable simulations using Version 1 of the CESM (which uses the Community Atmosphere Model Version 5, or CAM5, as its atmospheric component). They found that the simulated GFS climatology was of comparable or higher quality to those with CESM1, except for cloud cover and radiative properties. The GFS-simulated global shortwave and longwave cloud radiative effects were only about half as large as observed, with profound effects on the simulated planetary energy budget. Xiao et al. (2014) found that much of this response was attributable to inadequate cloud cover over most parts of the oceans, including the near-coastal part of the subtropical stratocumulus regions and tropical-subtropical shallow cumulus regions. On the other hand, one of the few regions in which cloud cover and radiative effects were overestimated in GFS is in the stratocumulus to cumulus transition regions, especially the East Pacific between the equator and 30° S; the model fails to accurately represent the coastal/open ocean contrast in cloud cover in addition to an global mean low bias. Thus, by focusing on the simulation of boundary layer clouds in the eastern subtropical oceans, we also hope to improve GFS-simulated cloud climatology in many other regions and globally averaged cloud radiative properties.

55 One focal strategy of the CPT is to use benchmark single-column model tests to identify possible
model improvements, which are then tested in short global integrations. This paper describes some
initial efforts to implement this strategy for improving GFS cloud simulations.

2 Method

We use GFS version 11.0.6 for both single column and global model experiments. The GFS single
60 column model (SCM) used in this study, as well as the forcing files, can be downloaded at <http://www.atmos.washington.edu/~jkg/GFS.SCM.html>, which also includes instructions for running the
SCM as well as routines modified for the experiments described in this paper. The global model may
be downloaded at http://www.nco.ncep.noaa.gov/pmb/codes/nwprod/sorc/global_fcst.fd/.

2.1 Single Column Modelling

65 The SCM has proven a useful tool in testing general circulation model (GCM) physics on properties
like clouds and precipitation in isolation from the effects of large-scale circulations (Randall et al.,
2003). GCM developers can use SCMs to compare model performance to that of high resolution
models such as large eddy simulation (LES) by running both with the same set of observationally-
derived forcings. These forcings specify the initial thermodynamic and wind profiles, the tendencies
70 of these profiles over the course of the simulation, and either the sea surface temperature or the
surface latent and sensible heat fluxes. As part of the GEWEX Cloud System Study (GCSS, now
subsumed into the Global Atmospheric System Study or GASS), a rich set of forcing cases exists
for this purpose, drawn from observational field campaigns encompassing different environments
ranging from nocturnal marine stratocumulus to continental deep convection (e.g., Siebesma et al.,
75 2003; Stevens et al., 2005; Grabowski et al., 2006).

The GFS has seldom been subject to this type of testing in the past, with developers generally
focusing on global model skill scores based on errors of meteorological variables such as 500 hPa
heights. Investigations of GFS physics that have used the single column modelling approach have
been oriented toward cirrus clouds and ice phase microphysics (e.g., Luo et al., 2005). In single-
80 column mode, we compare quantities relevant to the physics of warm boundary layer clouds, such
as cumulus updraught mass flux and thermodynamic properties, to those of identically forced LES,
using observationally-anchored cases. While single column modelling cannot substitute for sensitiv-
ity tests using 3D simulations, this method's relative simplicity and comparability with LES makes
it a useful tool for falsifying model physics and as a reference to guide interpretation of global model
85 results.

Our approach thus far in using SCM to improve model physics has been to identify components
of the parametrisations most relevant to boundary layer clouds that are a) formulated in ways that are
inconsistent with current knowledge of the process in question and b) possible sources of model bias.

We then aim to improve the component of the scheme while maintaining the general framework of
90 the parametrisation. In other words, while, for example, the “dual mass flux” scheme of Neggers
et al. (2009) is an attractive framework for unified parametrisation of large boundary layer eddies
and shallow convection, to implement this in the GFS would require a complete overhaul of both the
boundary layer and shallow convective schemes. Maintaining and improving the current framework
is a more pragmatic approach to improving GFS physics in the short term. In some cases, sensitivity
95 experiments comparing SCM to LES can identify sources of compensating errors, in which case
simultaneous improvements must be made to several aspects of the physical parametrisations to
reduce simulation biases.

The LES runs we compare to the SCM in this study use version 6 of the System for Atmospheric
Modeling (SAM, Khairoutdinov and Randall, 2003). In all runs, SAM resolves the largest boundary
100 layer eddies and all clouds, while smaller scale turbulence and microphysics are parametrised. SAM
has been included in LES intercomparison studies for the GCSS cases used here (Siebesma et al.,
2003; Stevens et al., 2005) and has been shown to reproduce observed precipitation, liquid water
path, surface fluxes, and cloud fraction (where such observations are available) in those cases, except
where we note otherwise.

105 **2.2 Global Model Experiments**

We also ran global model tests that complement our SCM experiments. Because global coupled
model experiments are far more computationally expensive than single column experiments, we
performed only three global experiments, with parameter changes chosen based partially on SCM
results and partially on simultaneous development strategies at NCEP.

110 As in Xiao et al. (2014), we use the NCAR Atmospheric Modeling Work Group/Working Group
on Numerical Experimentation diagnostic package (<http://www.cgd.ucar.edu/amp/amwg/diagnostics>)
to facilitate comparison of our global model experiments with observations.

3 Model Overview

This study is based on the 2011 version of GFS, the same as that used in the single column model. It
115 has a spectral triangular truncation of 126 waves (T126), equivalent to roughly one degree horizontal
grid spacing, and 64 hybrid sigma pressure levels (Sela, 2009). Compared with the previous version
of the GFS, the main changes are in the parametrisations of the shallow convection, the planetary
boundary layer (PBL), and deep convection (Han and Pan, 2011). Features of these schemes are
described in more detail in the next section.

120 This version of GFS uses the Atmospheric and Environmental Research Inc. Rapid Radiative
Transfer Model (RRTM) longwave parametrisation (Mlawer et al., 1997). The shortwave parametri-
sation is modified from the National Aeronautics and Space Administration (NASA) Goddard Space

Flight Center solar radiation scheme (Hou et al., 2002; Chou et al., 1998). Both radiation schemes assume maximum random cloud overlap.

125 The microphysics scheme (Zhao and Carr, 1997; Moorthi et al., 2001) prognoses cloud water specific humidity and cloud fraction following Sundqvist (1978). Both stratiform cloud processes and detrained cumulus cloud ice and condensate are sources of total cloud water.

For global simulations presented below, the GFS is coupled to the Modular Ocean Model 4 (MOM4), a finite difference version of the ocean primitive equations (Griffies et al., 2005). The
130 zonal resolution is 1/2 degree. The meridional resolution gradually decreases from 1/4 degree near the equator to 1/2 degree at high latitudes. There are 40 height layers, whose vertical spacing increases from 10 m near the surface to about 500 m in the bottom.

4 Physics parametrisations

This section summarizes the GFS shallow convection, planetary boundary layer (PBL), and cloud
135 fraction parametrisations, focusing on aspects relevant to our sensitivity tests. More detailed descriptions of these schemes are given by Troen and Mahrt (1986), Hong and Pan (1996), and Han and Pan (2011).

4.1 Shallow Convection

The GFS shallow cumulus scheme (Han and Pan, 2011) is a bulk entraining plume mass flux
140 parametrisation based on the GFS deep convection scheme (Pan and Wu, 1995; Han and Pan, 2011), but with new formulations of lateral entrainment and detrainment rate, a different mass-flux closure, and different plume microphysics.

The bulk plume originates from and shares the properties of the level of highest moist static energy (MSE) in the boundary layer, usually the lowest model level. It rises to its lifted condensation level,
145 where its mass flux is determined using the Grant (Grant and Brown, 1999) closure. The plume mass flux m is given by the equation

$$\frac{1}{m} \frac{dm}{dz} = \epsilon - \delta, \quad (1)$$

where ϵ is the fractional lateral entrainment rate and δ the fractional detrainment rate. The former is assumed to have the form $\epsilon = c/z$, where c is an adjustable nondimensional constant. The fractional
150 detrainment rate δ is constant with height and equal to the fractional entrainment rate at the height of cloud base. This ensures a mass flux profile that decreases with height within the cumulus updraft, consistent with the LES study of Siebesma and Cuijpers (1995). It also means that changes to c affect the detrainment rate as well as the entrainment rate. The same entrainment rate is used in determining the moist static energy and total water specific humidity (and hence the buoyancy) of
155 the cumulus updraught, as well as its horizontal velocity, relevant for cumulus momentum transport.

The bulk plume microphysics are simple: updraught liquid water is converted to precipitation (which falls down through the plume and can evaporate in the subcloud layer), and it is detrained to grid scale cloud condensate, both at rates proportional to the updraught liquid water content, following Lord (1978):

$$160 \quad q_c^{prec} \propto c_0 q_c^{cu} \quad (2)$$

and

$$q_c^{detr} \propto c_1 q_c^{cu}. \quad (3)$$

The scheme contains a flag that turns off shallow convection if the cloud top (constrained to a model level) is below the model-diagnosed PBL top, diagnosed with a bulk Richardson number. This ensures that clouds that lack the buoyancy to penetrate the inversion are handled entirely by the PBL scheme rather than the shallow convection scheme. In the operational GFS, this flag is commented out because it has little impact on NCEP’s traditional forecast skill metrics. Our tests, discussed below, showed that this may nevertheless often be important to the parametrised boundary-layer cloud cover and precipitation.

170 Shallow cumulus cloud top is determined by cloud work function (Arakawa and Schubert, 1974), i.e., the vertically integrated buoyancy of the entraining updraught. Updraughts are given energy equal to 10% of cloud work function to overshoot their level of neutral buoyancy. We test an alternative formulation of cloud top that instead uses an equation for the square of the cumulus updraught vertical velocity w :

$$175 \quad \frac{1}{2} \frac{d(w^2)}{dz} = aB - b\epsilon w^2, \quad (4)$$

where a and b are tunable parameters and B is the cumulus updraught buoyancy. Choosing the parameters such that $b/a > 1$ roughly parametrises the effect of perturbation pressure gradients on vertical velocity (Bretherton et al., 2004).

180 Key parameters in the shallow convection scheme that affect its performance include the fractional entrainment/detrainment parameter c used in Eq. 1 and the rates c_0 and c_1 in Eqs. 2 and 3, respectively. If Eq. 4 is used to determine cloud top, then a and b may also be important parameters.

4.2 PBL turbulence and stratiform clouds

The GFS boundary layer turbulence parametrisation (Hong and Pan, 1996) is an eddy diffusivity scheme modified from Troen and Mahrt (1986) with an added “countergradient” term (for temperature only) representing the nonlocal mixing done by the largest PBL eddies. Han and Pan (2011) modified the turbulence scheme by adding a simple parametrisation of cloud top-driven mixing after Lock et al. (2000). This entrainment rate is proportional to the radiative flux jump across cloud top and represents cloud top cooling enhancement of boundary layer entrainment. The original Lock

scheme also parametrised mixing-induced buoyancy reversal; this process is not included in the GFS
190 scheme.

The operational GFS uses two different cloud fraction schemes: one for radiative flux calculations, the other for stratiform microphysics calculations. The radiation scheme uses the Xu and Randall (1996) fit of observed cloud fraction to relative humidity RH, condensate specific humidity q_l , and saturation specific humidity q_s :

$$195 \quad \sigma_{XR} = \text{RH}^{k_1} \left(1 - \exp \left\{ - \frac{k_2 q_l}{[(1 - \text{RH})q_s]^{k_3}} \right\} \right). \quad (5)$$

The model uses the original Xu and Randall (1996) empirical values for the fit parameters: $k_1 = 0.25$, $k_2 = 100$, $k_3 = 0.49$. However, the condensate specific humidity used is only that of the stratiform microphysics scheme. Thus, cumulus convection only interacts with radiation indirectly through its effect on large-scale temperature and moisture fields. The stratiform microphysics
200 scheme is derived from Sundqvist (1978) and parametrises cloud fraction based on relative humidity in excess of a prescribed, latitudinally-varying critical RH. The cloud fraction used in the Sundqvist scheme affects the model indirectly through the autoconversion and large-scale condensation rates. To maintain consistency with the rest of the scheme the Sundqvist formulation must be used. However, the Xu and Randall scheme matches observations better in general and is preferable for the
205 radiation scheme. CPT members at NCEP are developing a single cloud fraction scheme to be used throughout the model in future GFS versions.

5 Single column results

5.1 Model setup

The SCM is based on the operational version of the GFS, including the same 64 vertical levels,
210 with vertical spacing in the PBL of 50-100 m. We run the SCM with a five-minute time step (half that used in the global simulations we present later in this paper), but the radiation scheme is called once per hour as in the GFS. In single column mode, horizontal tendencies in wind, temperature, and moisture fields are prescribed by the forcing file in place of large-scale dynamics. The winds at each level are also forced by Coriolis and pressure-gradient forces, taking the initial wind profile as
215 the geostrophic wind. The SCM's physical parametrisations are identical to those of the operational GFS except for options to include a few minor modifications planned for future GFS versions. These are discussed below and evaluated in our sensitivity experiments. Our single column sensitivity tests use two GCSS cases, described below.

5.2 BOMEX

220 For sensitivity tests to changing parameters in the shallow convection scheme, we utilize a non-precipitating quasi-steady oceanic shallow cumulus case presented by Siebesma et al. (2003), de-

rived from the Barbados Oceanographic and Meteorological Experiment (BOMEX, Holland and Rasmusson, 1973). The specified forcings already include the effects of radiative cooling, and cloud-radiation interaction is not considered in this case, so the radiation schemes are turned off
225 in the SCM and the LES.

5.2.1 Experiment description

We use the BOMEX case to study model sensitivity to changing aspects of the shallow convection scheme. In accordance with the discussion in Section 3b, we test model sensitivity to changing several parameters. These parameter changes are summarized on Table 1. First, in the *ShCuCldCover*
230 experiment, we include cumulus updraught condensate in the cloud fraction parametrization (eqn 5). This change is included in subsequent experiments as well.

Second, we test sensitivity to the updraught lateral entrainment rate, parametrised as $\epsilon = c/z$. We run experiments with LES-compatible choices of c in the range of 1.0-2.0 (Siebesma et al., 2003) instead of the operational value $c = 0.3$. Because the GFS parametrises updraught detrainment rate
235 as constant with height and equal to the entrainment rate at cloud base (where it is maximum within the cloud), changing c also changes the detrainment rate. For this reason, we will henceforth refer to c as the entrainment/detrainment parameter.

At the same time, we test sensitivity to the efficiency of conversion of updraught condensate into precipitation or detrained condensate. The operational GFS converts updraught condensate in a grid
240 layer to precipitation and detrains it to grid scale condensate at rates given in Eqs. 2 and 3; both rates are proportional to the condensate mixing ratio. This means that any updraught condensate is precipitated out over an e-folding depth of 400 m, causing extremely efficient precipitation even from the shallowest cumulus clouds. In practice, this compensates for the inadequate dilution of updraught condensate by lateral mixing, as we describe further below. In configuration *NewEntr*,
245 we decreased these rates – in combination with increases to entrainment – to $c_0 = 0.001 \text{ m}^{-1}$, $c_1 = 2.5 \times 10^{-4} \text{ m}^{-1}$. This can be regarded as an intermediate step toward the LES results: in *NewEntr* the lateral entrainment rate is still underestimated, compensated by overestimation of conversion of updraught condensation to precipitation, but both compensating errors are much smaller than with the operational parameter choices.

250 Lastly, we also show the effect of using the vertical velocity eqn 4 to determine cloud top. We show the effect of this change both without the *NewEntr* change (*VvelOrig*) and with it (*VvelNewEntr*).

5.2.2 Results

Our initial sensitivity tests only involved single parameter changes. This quickly uncovered compensating errors – multiple parameters incorrectly tuned such that their effects cancel each other –
255 in the shallow cumulus scheme. For example, only increasing the updraught lateral entrainment rate resulted in a simulation with an improved mass flux profile but far too small updraught condensate

amount, while only decreasing the precipitation and detrainment conversion rates reduced excess precipitation but produced too much condensate. Furthermore, only reducing one of c_0 or c_1 simply shifts precipitation between the shallow convection and stratiform microphysics schemes, with little
260 reduction in overall precipitation. It is necessary to change all of these parameters together in order to address these compensating errors, so we only show results from simulations in which multiple parameters were changed.

Figure 1 shows profiles of liquid water potential temperature and total water specific humidity averaged over hours 3-6 of the BOMEX experiments. We show these primarily to give the reader
265 a sense of the environment being simulated: a fairly well-mixed subcloud layer up to about 500 m, a conditionally unstable cloud layer, and a capping inversion starting slightly above 1400 m. SCM results differ from LES primarily in a less well-mixed subcloud layer, a more stably stratified cloud layer, and excess moisture at the inversion. This last feature is explored more in the forthcoming discussion. Biases are most extreme in the *VvelOrig* configuration, with profiles that imply far too
270 much mixing with the free troposphere.

A major problem with the control GFS simulation of the BOMEX case is that it over-precipitates. The BOMEX case is idealized, but it is designed to mimic a several-day period during which observers and photographs suggest precipitation was negligible (Siebesma and Cuijpers, 1995), consistent with our LES results. Figure 2a shows time series of surface precipitation for the experiments.
275 The control configuration maintains a convective precipitation rate of 1.5 mm day^{-1} , large enough to be a sizeable moisture sink to the trade cumulus boundary layer, compensating roughly 30% of the surface evaporation. *NewEntr* reduces the convective precipitation by 60%, but does not eliminate the problem because the precipitation flux is still proportional to the updraught condensate specific humidity, ensuring that all shallow convection will precipitate at least a little.

The *VvelOrig* configuration actually worsens the bias. Later we show that this is due to an overdeepening of cumulus convection. However, in combination with *NewEntr*, the spurious precipitation is reduced and the shallow convection scheme is prevented from switching off and on as it does in the non-*Vvel* experiments.
280

Figure 2 shows that all configurations maintain very small liquid water path for the first few hours
285 of simulation. This is because nearly all the cloud water is associated with the shallow convection scheme. At varying times in the simulation, however, the LWP rapidly increases in the *Control*, *ShCuCldCover*, and *NewEntr* experiments. This indicates rapid development of stratiform cloud, which only the *Vvel* change is able to prevent.

Figure 3 shows profiles of stratiform cloud water and cloud fraction from both the stratiform
290 microphysics scheme and the radiation scheme. In the left panel, we see that most of the stratiform condensation responsible for the rise in LWP in Fig. 2b occurs at one model level near cloud top. The reasons for this will be explored below. The right panel shows that simply adding cumulus condensate to the radiation cloud fraction – the *ShCuCldCover* change – is a major improvement,

though the bias is now too much cloud cover rather than too little. This bias is reduced by subsequent
295 parameter changes, and the spike in upper PBL cloud cover (and condensate) is removed by the *Vvel*
change. Finally, comparing the middle and right panels shows the large difference that can exist
between cloud fraction in the microphysics scheme and that of the radiation scheme.

Figure 4 shows time-averaged cumulus updraught properties: mass flux and condensate specific
humidity. For the LES comparison, we define cumulus updraught properties as the average across
300 all LES grid points that are both saturated and have positive vertical velocity.

The mass flux profiles of the *Control* and *ShCuCldCover* configurations show the effect of those
experiments' high precipitation. Evaporation of rainfall below cloud base overstabilizes the subcloud
layer, reducing cumulus updraught buoyancy such that convection often extends only one or two
grid levels above cloud base – if it isn't shut off completely. This leads to a time-averaged mass flux
305 profile that is too bottom-heavy and biased low, particularly between 800 and 1200 m. However, the
cloud top is in good agreement with LES.

The *NewEntr* parameter change improves on this by reducing precipitation directly (via the pre-
cipitation efficiency c_0) and indirectly (via increased entrainment dilution and reduced mass flux in
the upper cloud layer). However, the cloud top is lower than the *Control* configuration and LES –
310 this is also due to increased entrainment dilution. The tendency of the GFS to produce too-low shal-
low cumulus cloud top when the entrainment rate is set to a value suggested by current knowledge
is in fact why the operational value of c is so small.

The *Vvel* parameter change increases cloud depth and enhances penetrative entrainment of warm
dry inversion air. This is what prevents stratiform condensation in the *Vvel* runs. With the operational
315 settings for c , c_0 , and c_1 , the bias is over-corrected, with cloud top that is far too high. However, in
combination with the *NewEntr* change, substantial improvement in the mass flux profile – as well as
those shown in previous figures – is seen.

Finally, the right panel of Fig. 4 demonstrates the compensating errors at work in the shallow
convection scheme. All configurations produce similar values for cumulus updraught condensate
320 specific humidity, values that are close to that of LES. They do so via different tradeoffs between
precipitation and entrainment. A major aspect of our parameter changes has aimed to shift the
removal of updraught liquid water content away from precipitation and toward increased mixing
with the free troposphere.

5.3 DYCOMS

325 To study model behavior in a stratocumulus environment, we use a case distilled from the Dynamics
and Chemistry of Marine Stratocumulus (DYCOMS-II, referred to hereafter as DYCOMS) Research
Flight 1, which sampled a nocturnal, nonprecipitating, well-mixed marine stratocumulus boundary
layer under a strong capping inversion in the Northeast Pacific (Stevens et al., 2003). We use the
GCSS DYCOMS case forcings as presented by Stevens et al. (2005) and Zhu et al. (2005). However,

330 those studies used an idealized longwave radiation code in their simulations; we use the full model
(longwave only) radiation code in both SCM and LES.

5.3.1 Experiment description

We found in our *Control* DYCOMS simulation that the shallow cumulus scheme was transporting
much of the heat and moisture through the PBL despite this being a stratocumulus case (not shown).
335 Recall from section 3b that there is a logical flag within the shallow convection scheme code that
turns shallow convection off if the cumulus cloud top is at or below PBL top. Thus, in bound-
ary layers where moist updraughts have insufficient energy to penetrate the capping inversion, PBL
cloudiness and entrainment will be handled by the PBL scheme rather than the cumulus convection
scheme. This flag is not used by default, even though it is physically reasonable, but we experi-
340 mented with using it, effectively turning convection off for the duration of the run. This "ShCuFlag"
experiment is shown along with the configurations already shown for the BOMEX case. The excep-
tion to this is the *ShCuCldCover* configuration, which has no effect on the DYCOMS case and is not
shown here.

The operational GFS also includes a minimum background diffusion applied both in and above
345 the PBL. The background diffusivity for heat and moisture in the operational GFS decreases expo-
nentially with height from $1.0 \text{ m}^2\text{s}^{-1}$, giving rise to about $0.9 \text{ m}^2\text{s}^{-1}$ at the 900 hPa level, a typical
PBL top in marine stratocumulus. To reduce erosion of coastal stratocumulus, NCEP developers
have further reduced the lower inversion layers' background diffusivity; it is now 30% of that at the
surface (i.e., $0.3 \text{ m}^2\text{s}^{-1}$; Han and Pan, 2011). Hence, we use this reduced background diffusivity in
350 our DYCOMS simulations.

5.3.2 Results

All DYCOMS experiments with the GFS maintain a reasonably strong capping inversion, given the
model resolution, and produce cloud fraction of about 1.0 after initial spinup (not shown). In this
respect, the DYCOMS SCM simulations do not have the same biases that the global coupled model
355 shows in the Northeast Pacific, where the model generates too shallow boundary layer and too low
cloud fraction. This limits the interpretation of SCM results.

Figure 5 shows the evolution of precipitation and LWP. As noted by Stevens et al (2005), LES
models tend to underestimate LWP in the DYCOMS case, which was observed to be about 60 g
 m^{-2} . The SCM LWP is actually closer to observations. However, this is achieved with a drizzle
360 rate of roughly 0.5 mm d^{-1} . Both observations (Stevens et al., 2003) and LES indicated no drizzle
at the surface or even at cloud base. Thus it appears that, as with the convection scheme, the physics
parametrisations controlling stratocumulus are too tuned toward precipitation as a mechanism for
PBL drying. The simplest explanation is that the modified Lock et al. (2000) parametrisation in the
SCM is not producing enough cloud top entrainment of warm, dry air. Initial results, to be reported in

365 a future study, indicate that increasing the entrainment rate in the Lock scheme while simultaneously decreasing the autoconversion rate in the stratiform microphysics scheme can maintain observed LWP while reducing excess precipitation in the DYCOMS simulation.

The most obvious differences are between 1) the *Control* and *NewEntr* experiments, and 2) the ShCuFlag and *Vvel* experiments. As part of the implementation of using vertical velocity for cloud top prediction, a logical flag turning off shallow convection if it is less than 70 hPa deep is included. Thus, the *Vvel* configurations look just like the ShCuFlag configuration because all of them result in the model turning off shallow convection. Fig. 5 shows that, without shallow convection, the model takes 2.5 hours to spin up cloud LWP despite having a five-minute time step and having been initialized with a supersaturated moisture profile. However, experiments with a different stratocumulus case (not shown) show that this is not the case if the model is initialized with liquid water, and furthermore initializing with liquid water eliminates the oscillations that are seen when the shallow convection scheme is active. These oscillations result from convective precipitation stabilising the subcloud layer and reducing convective mass flux, and hence detrained convective condensate, in the subsequent time step.

380 6 Global model results

6.1 Configuration and experiment description

We perform four simulations with the global version of GFS coupled to MOM4: a 50-year run with GFS operational settings; a one-year control run that, apart from length, is identical to the 50-year run; and two one-year sensitivity experiments: *shortrun1* and *shortrun2*. *Shortrun1* includes most of the parameter changes to the shallow convection scheme suggested by our BOMEX SCM study. *Shortrun2* also includes changes suggested by the DYCOMS study and by basic physical considerations not exposed by either SCM case. All experiments are identically initialized on January 1st, 1948. The atmosphere is initialized by NCEP-NCAR reanalysis (Kalnay et al., 1996); the ocean is initialized with the Climate Forecast System Reanalysis (Saha et al., 2010), and the initial state is neutral with respect to the NINO3.4 (El Nino/Southern Oscillation) index. We included ocean-coupling for two reasons. First, it corresponds to the setup for seasonal climate prediction, an important application of GFS. Second, it was easier for us to set up a coupled simulation than an uncoupled simulation with seasonally varying SSTs.

The parameter changes in *Shortrun1* and *Shortrun2* are summarized in Table 2. *Shortrun1* increases the lateral entrainment rate and reduces the rain conversion rate in the shallow convection parametrisation, following two of the three prescriptions in the BOMEX *NewEntr* case. *Shortrun2* also reduces the condensate detrainment rate (the other parameter change made in *NewEntr*), uses cumulus condensate for cloud fraction, and uses the vertical velocity eqn 4 for cloud top. *Shortrun2* also incorporates the additional changes discussed in the DYCOMS ShCuFlag case: to prevent shal-

400 low convection with a cloud top that does not extend above the PBL top and to decrease background diffusion in inversion layers. However, the former might have little impact in combination with the vertical velocity cloud top change, as was seen in the DYCOMS simulations.

For physical correctness, a parametrisation of heating due to turbulent kinetic energy (TKE) dissipation is included. We expect this to have negligible impact on any SCM simulation of existing 405 subtropical boundary layer cloud cases. Viscous dissipation of TKE can be a significant source of heat, especially in strong wind conditions such as in hurricanes (Bister and Emanuel, 1998). Although not shown in this paper, inclusion of TKE dissipative heating not only increased the 10-meter maximum wind about 10-30% in hurricane forecasts, but also largely reduced the unexplained GFS atmospheric energy loss of about $4\text{-}5 \text{ W m}^{-2}$. These results will be presented in a forthcoming 410 paper; they have little effect on subtropical boundary layer clouds.

For the following discussion we focus on marine low cloud sensitivity in the southeastern Pacific for September-October-November (SON). Even though this is only 9-11 months after the start of the simulations, the climatological marine low cloud bias and its sensitivity to parameter changes has already emerged, as can be seen by comparing Figures 6a (the one-year run) and 6d (the 50- 415 year run). Cloudiness differences driven by synoptic timescale variability in the southeastern Pacific may affect the exact magnitudes of changes in the bias in the sensitivity experiments; by comparing the differences between the simulations in the three individual months comprising the SON period (not shown) we are confident that the signals we report are robust to synoptically-driven cloudiness fluctuations.

420 6.2 Results

Figures 6-7 show the sensitivity of shortwave cloud radiative effect (SWCRE) and low cloud fraction over the Pacific region for SON. In these plots, panel (a) shows the bias of the control simulation compared to satellite-derived climatologies, and the next two panels show the difference of the control from the two sensitivity runs. The observations used in Fig. 7a are a combination of the 425 climatological low cloud fraction from the CLOUDSAT/CALIPSO GEOPROF product (Kay and Gettelman, 2009) and the CALIPSO GOCCP product (Chepfer et al., 2010) for 2006-2010—in each grid box the maximum low cloud fraction from the two is used. This method enhances the low cloud fraction just off the west coasts of the American and African continents because GEOPROF tends to underestimate low cloud amount because it screens out clouds with tops below 500 m altitude. However, 430 GEOPROF is more accurate in general because the combination of CLOUDSAT and CALIPSO instruments can detect low clouds better when mid- and high-level clouds are present. The SWCRE observation used in Fig. 6a and 6d is from the Clouds and Earth's Radiant Energy System Edition 2 (CERES2, Minnis et al. 2011) for 2000-2005. In these panels, biases on the *Control* simulation are reduced where the colours indicate differences of the same sign as the upper panel (e. g. blue 435 colours where there is a blue colour in the upper panel, or vice versa).

While it would be ideal to compare model simulations to observations over the same time period, we found it technically much simpler to initialise the short GFS runs with the same initial conditions as the 50-year run rather than with initial conditions from the satellite era. Long-term trends and decadal variability in global mean downwelling surface radiation are on the order of
440 $+0.25 \text{ W m}^{-2}$ and $\pm 3\text{-}5 \text{ W m}^{-2}$, respectively (Hinkelman et al., 2009), one to two orders of magnitude smaller than the GFS shortwave bias. Additionally, the decade 2000-2010 was one of weak ENSO variability (<http://www.esrl.noaa.gov/psd/enso/mei/>). This gives us confidence that the difference in decades for which we compare means will not substantially affect our results.

In the southeastern Pacific, *Control* shows large positive errors of SWCRE (Fig. 6a) near the
445 South American coast and negative errors further offshore, which corresponds clearly to the errors in marine low clouds (Fig. 7a), as discussed in Xiao et al. (2014). *Shorrun1* (Figs. 6b and 7b) shows small but consistent reduction of errors in low cloud fraction (less than 10%) and SWCRE (less than 10 W m^{-2}) both near the South American coast and in the open ocean, while *Shorrun2* shows similar patterns of error reduction but with much larger amplitude – $20\text{-}30 \text{ W m}^{-2}$ for SWCRE. In the
450 tropics ($15^{\circ}\text{S}\text{-}15^{\circ}\text{N}$), the overextension of low clouds onto the equator from the southeastern Pacific is also reduced in *Shorrun2*. There is also a large reduction of SWCRE errors in the Inter-Tropical Convergence Zone (ITCZ) and South Pacific Convergence Zone (SPCZ) in *Shorrun2*, which we will discuss in more detail together with the SST response later in this section. The global mean SWCRE bias in *Shorrun2*, compared to that in *Control*, is reduced by about half, from 23 W m^{-2}
455 to 11 W m^{-2} for the annual average of 1948 minus the CERES2 annual mean from 2000-2005; this bias reduction occurs persistently throughout the year.

Figure 8 shows the sensitivity of low cloud structure along 20°S in the East and Central Pacific for SON. In *Control* (Fig. 8b), the lack of clouds near the coast and the overextension offshore is clear in comparison to the CERES2-MODIS-CALIPSO-CLOUDSAT (CCCM) dataset from the
460 Atmospheric Science Data Center at NASA Langley Research Center, Fig. 8a.

In *Shorrun1* (Fig. 8c), the stratocumulus layer gets slightly thinner in general but the maximum in cloud water content increases and remains too far offshore, making the total error reduction small. This is likely because decreasing the shallow cumulus precipitation efficiency c_0 without changing the condensate detrainment rate c_1 simply shifts the shallow convective condensate sink from precipitation to detrainment to grid scale cloud. *Shorrun2* (Fig. 8d), on the other hand, shows reduced
465 cloud water content offshore and increased cloud water close to the coast, more consistent with observations. However, the cloud layer in *Shorrun2* extends too deep and the trade-wind inversion is weakened (not shown). Furthermore, both *Shorrun1* and *Shorrun2* show excessive cloud liquid water compared to CCCM in the trade cumulus regime extending across the westernmost part of the
470 cross-section, worsening a bias already present in control.

The cloud structure changes can be related to changes in the behavior of the parametrised shallow convection. Figure 9 shows heating and moistening from the shallow convection scheme in each ex-

periment along the transect. The difference between *Shorrun2* and *Shorrun1* east of 100°W shows that nearly all shallow convective activity has been eliminated in this region, which is observed to
475 be dominated by stratocumulus clouds. Meanwhile, increasing the entrainment/detrainment parameter (one of the two differences between *Shorrun1* and *Control*) decreases mass flux in the upper cloud layers and thus reduces convective heating in the cumulus and Sc-Cu transition regions west of 100°W.

The SST response in SON is shown in Figure 10 for *Shorrun2*. The response in *Shorrun1* is
480 small and not shown here. In *Control*, we see large positive SST errors near the American coasts (4°C off South American coast) and negative biases to their west (-2°C in the southeastern Pacific). In the tropics, there are warm SST biases of 2°C along the ITCZ and SPCZ and near the maritime continent, and negative biases along the equator. In *Shorrun2*, the negative biases in the southeastern Pacific are reduced by at least half but the warm biases near the coast are worsened. In the tropics the
485 warm biases along ITCZ and SPCZ and near the maritime continent are reduced, but the equatorial cold bias is turned into a warm bias, especially between 150 – 180°W.

It is unlikely that changes in cloud radiative forcing directly caused the SST changes in deep convective regions, where the substantial change in shortwave cloud forcing was largely offset by a change in longwave cloud forcing (not shown). However, reductions in excess cloud cover in
490 the offshore southeast Pacific may contribute to the increase in SST in that region and subsequent reduction in zonal SST gradient associated with a weakening of the Walker circulation. This can also be seen in the change in SST off the Peruvian and Chilean coasts, where positive SST biases worsen despite an increase in cloud cover. This is likely due to a weakening in coastal upwelling. We found that changes in wind stress also suggest a weakening of this circulation, with a decrease
495 in surface easterlies in the central and west Pacific and a reduction of northerlies in the southeast Pacific (not shown). Such sensitivity of the basin-wide Hadley-Walker circulation pattern to changes in marine low clouds associated with parameter changes in shallow convection and moist turbulence parametrisation is also found in other GCMs (e.g., Ma et al., 1994; Xiao et al., 2014).

7 Future tests

500 While testing parametrisation changes in climate mode for the GFS is an important aspect of our work, parameterisation development requires testing model changes effect on forecast skill as well. Typically, data assimilation tests with runs of at least two months are done. If forecast skill is improved, especially in terms of the 500 hPa anomaly correlation, precipitation skill over the United States, or hurricane track forecast, the change is likely to be implemented. If the skill is neutral but
505 the climate bias is reduced, there is still a good chance of implementing the change. If the forecast skill is degraded, modifications or re-tuning of other model parameters, such as those controlling autoconversion or the critical relative humidity used for condensation, will be tried.

A short data assimilation experiment implementing the model changes included in the *NewEntr* and *ShCuCldCover* SCM results of BOMEX and DYCOMS, respectively, has been performed. Initial results suggest that, while in many respects the forecast skill is improved or neutral, the root mean square error in tropical horizontal winds is increased. As a consequence of these experiments, further work must be done before these changes can be implemented into future versions of the GFS; climate improvements must, at the very least, have a neutral impact on forecasts. Single column tests (not shown) indicate that changes in horizontal winds are not a result of cumulus momentum transport – the *NewEntr* change has no impact on winds in the SCM. Instead, the change is affecting horizontal pressure gradients; thus more global model tests – and possible model-retuning – are needed to investigate this further. This work is underway by NCEP developers and will be reported on in a future study.

8 Conclusions

The NOAA stratocumulus-to-cumulus transition Climate Process Team has run sensitivity experiments to single-column and global coupled versions of the NCEP-GFS model in conjunction. To improve the GFS simulation of subtropical boundary layer cloud, we used single-column simulations to identify and attribute underlying problems in the shallow convection scheme, and we then tested improvements suggested by this approach in short global coupled simulations.

In single-column mode, we found that some simple parameter changes to the shallow convection scheme improved simulated boundary-layer structure and precipitation compared to LES. In particular, it is beneficial to increase cumulus lateral mixing with the environment and decrease the rate at which updraught condensate falls out as rain and is detrained to the grid scale. This shifts some of the cumulus updraught removal of water from precipitation to evaporation associated with entrainment.

However, the single-column model still over-precipitates in both shallow convective and stratiform environments. We hypothesize that this can be improved by increasing entrainment of warm, dry free-tropospheric air into the boundary layer through changes to the boundary layer scheme, by reducing autoconversion of liquid cloud water to rain in the stratiform microphysics scheme, and by reformulating shallow convective precipitation to suppress all rainfall when condensate specific humidity is small.

One-year global coupled model experiments combining these changes substantially reduce biases in subtropical low cloud fraction and shortwave cloud forcing seen in the control version of GFS. Improvements are seen in the deep convective regions as well as the subtropical boundary-layer cloud regimes. Global model changes also improve SST and precipitation bias in most regions. However, underestimation of low cloud off the subtropical west coasts of the Americas remains a problem even after the changes, and increased tropical wind RMSE must be addressed before this

change can be implemented in the GFS.

545 The CPT's focus has been improving cloud regimes associated with the stratocumulus to trade
cumulus transition. As we continue our GFS development efforts, we will take a more holistic
approach, focusing on better simulation of global cloud cover and its radiative effects through im-
provements of the microphysics, cloud fraction, cumulus convection, and PBL parametrisations and
their interactions.

Acknowledgements. This work is supported by NOAA MAPP grant GC10-670a as part of the Sc-Cu Climate
550 Process Team. The first author would like to thank Dr. Hua-Lu Pan at NCEP for his support and Dr. Peter
Blossey at University of Washington for providing LES runs.

References

- Arakawa, A. and Schubert, W. H.: Interaction of a cumulus cloud ensemble with the large-scale environment, *Journal of the Atmospheric Sciences*, 31, 674–701, doi:http://dx.doi.org/10.1175/1520-0469(1974)031%3C0674:ioacce%3E2.0.co;2;10.1175/1520-0469(1974)031<0674:ioacce>2.0.co;2, (GotoISI)://WOS:A1974S778800004, 1974.
- 555
- Bister, M. and Emanuel, K. A.: Dissipative heating and hurricane intensity, *Meteorology and Atmospheric Physics*, 65, 233–240, 1998.
- Bretherton, C. S., McCaa, J. R., and Grenier, H.: A new parameterization for shallow cumulus convection and its application to marine subtropical cloud-topped boundary layers. Part I: Description and 1D results, *Monthly Weather Review*, 132, 864–882, doi:http://dx.doi.org/10.1175/1520-0493(2004)132%3C0864:anpfsc%3E2.0.co;2;10.1175/1520-0493(2004)132<0864:anpfsc>2.0.co;2, (GotoISI)://WOS:000220450000002, 2004.
- 560
- Chepfer, H., Bony, S., Winker, D., Cesana, G., Dufresne, J. L., Minnis, P., Stubenrauch, C. J., and Zeng, S.: The GCM-Oriented CALIPSO Cloud Product (CALIPSO-GOCCP), *Journal of Geophysical Research-Atmospheres*, 115, doi:http://dx.doi.org/10.1029/2009jd012251.1029/2009jd012251, (GotoISI)://WOS:000275304600002, 2010.
- 565
- Chou, M. D., Suarez, M. J., Ho, C. H., Yan, M. M. H., and Lee, K. T.: Parameterizations for cloud overlapping and shortwave single-scattering properties for use in general circulation and cloud ensemble models, *Journal of Climate*, 11, 202–214, doi:http://dx.doi.org/10.1175/1520-0442(1998)011%3C0202:pfcoas%3E2.0.co;2;10.1175/1520-0442(1998)011<0202:pfcoas>2.0.co;2, (GotoISI)://WOS:000072156100006, 1998.
- 570
- Grabowski, W. W., Bechtold, P., Cheng, A., Forbes, R., Halliwell, C., Khairoutdinov, M., Lang, S., Nasuno, T., Petch, J., Tao, W. K., Wong, R., Wu, X., and Xu, K. M.: Daytime convective development over land: A model intercomparison based on LBA observations, *Quarterly Journal of the Royal Meteorological Society*, 132, 317–344, doi:http://dx.doi.org/10.1256/qj.04.14710.1256/qj.04.147, (GotoISI)://WOS:000236697900004, 2006.
- 575
- Grant, A. L. M. and Brown, A. R.: A similarity hypothesis for shallow-cumulus transports, *Quarterly Journal of the Royal Meteorological Society*, 125, 1913–1936, doi:http://dx.doi.org/10.1256/smsqj.5580110.1256/smsqj.55801, (GotoISI)://WOS:000082254800001, 1999.
- 580
- Griffies, S. M., Gnanadesikan, A., Dixon, K. W., Dunne, J. P., Gerdes, R., Harrison, M. J., Rosati, A., Russell, J. L., Samuels, B. L., Spelman, M. J., Winton, M., and Zhang, R.: Formulation of an ocean model for global climate simulations, *Ocean Science*, 1, 45–79, (GotoISI)://WOS:000208484900006, 2005.
- 585
- Han, J. and Pan, H.-L.: Revision of Convection and Vertical Diffusion Schemes in the NCEP Global Forecast System, *Weather and Forecasting*, 26, 520–533, doi:http://dx.doi.org/10.1175/waf-d-10-05038.1.10.1175/waf-d-10-05038.1, (GotoISI)://WOS:000294244200006, 2011.
- 590
- Hinkelman, L. M., Stackhouse Jr., P. W., Wielicki, B. A., Zhang, T., and Wilson, S. R.: Surface insolation trends from satellite and ground measurements: Comparisons and challenges, *Journal of Geophysical Research*, 114, 1–18, doi:http://dx.doi.org/10.1029/2008JD011004.1029/2008JD011004, 2009.
- Holland, J. Z. and Rasmusson: Measurements of atmospheric mass, energy, and momentum bud-

- gets over a 500-kilometer square of tropical ocean, *Monthly Weather Review*, 101, 44–55, doi:[http://dx.doi.org/10.1175/1520-0493\(1973\)101%3C0044:motame%3E2.3.co;2](http://dx.doi.org/10.1175/1520-0493(1973)101%3C0044:motame%3E2.3.co;2), <GotoISI>://WOS:A1973P298400005, 1973.
- 595 Hong, S. Y. and Pan, H. L.: Nonlocal boundary layer vertical diffusion in a Medium-Range Forecast Model, *Monthly Weather Review*, 124, 2322–2339, doi:[http://dx.doi.org/10.1175/1520-0493\(1996\)124%3C2322:nblvdi%3E2.0.co;2](http://dx.doi.org/10.1175/1520-0493(1996)124%3C2322:nblvdi%3E2.0.co;2), <GotoISI>://WOS:A1996VL88800012, 1996.
- Hou, Y., Moorthi, S., and Compana, K.: Parameterization of solar radiation transfer in NCEP models, NCEP
600 Office Note, 441, <http://www.emc.ncep.noaa.gov/officenotes/FullTOC.html#2000>, 2002.
- Kalnay, E., Kanamitsu, M., Kistler, R., Collins, W., Deaven, D., Gandin, L., Iredell, M., Saha, S., White, G., Woollen, J., Zhu, Y., Chelliah, M., Ebisuzaki, W., Higgins, W., Janowiak, J., Mo, K. C., Ropelewski, C., Wang, J., Leetmaa, A., Reynolds, R., Jenne, R., and Joseph, D.: The NCEP/NCAR 40-year reanalysis project, *Bulletin of the American Meteorological Society*, 77, 437–471, doi:[http://dx.doi.org/10.1175/1520-0477\(1996\)077%3C0437:tnyrp%3E2.0.co;2](http://dx.doi.org/10.1175/1520-0477(1996)077%3C0437:tnyrp%3E2.0.co;2), <GotoISI>://WOS:A1996UG17600001, 1996.
- 605 Kay, J. E. and Gettelman, A.: Cloud influence on and response to seasonal Arctic sea ice loss, *Journal of Geophysical Research: Atmospheres* (1984–2012), 114, 2009.
- Khairoutdinov, M. F. and Randall, D. A.: Cloud resolving modeling of the ARM summer 1997 IOP:
610 Model formulation, results, uncertainties, and sensitivities, *Journal of the Atmospheric Sciences*, 60, 607–625, doi:[http://dx.doi.org/10.1175/1520-0469\(2003\)060%3C0607:crmota%3E2.0.co;2](http://dx.doi.org/10.1175/1520-0469(2003)060%3C0607:crmota%3E2.0.co;2), <GotoISI>://WOS:000180827200002, 2003.
- Lock, A. P., Brown, A. R., Bush, M. R., Martin, G. M., and Smith, R. N. B.: A new boundary layer mixing scheme. Part I: Scheme description and single-column model tests, *Monthly Weather Review*, 128, 3187–
615 3199, doi:[http://dx.doi.org/10.1175/1520-0493\(2000\)128%3C3187:anblms%3E2.0.co;2](http://dx.doi.org/10.1175/1520-0493(2000)128%3C3187:anblms%3E2.0.co;2), <GotoISI>://WOS:000089461100008, 2000.
- Lord, S.: Development and observational verification of cumulus cloud parameterization, Ph. D. Thesis, University of California, Los Angeles, 1978.
- Luo, Y. L., Krueger, S. K., and Moorthi, S.: Cloud properties simulated by a single-column model. Part I: Comparison to cloud radar observations of cirrus clouds, *Journal of the Atmospheric Sciences*, 62, 1428–1445, doi:<http://dx.doi.org/10.1175/jas3425.1>, <GotoISI>://WOS:000229335800009, 2005.
- 620 Ma, C. C., Mechoso, C. R., Arakawa, A., and Farrara, J. D.: Sensitivity of a coupled ocean-atmosphere model to physical parameterizations, *Journal of Climate*, 7, 1883–1896, doi:[http://dx.doi.org/10.1175/1520-0442\(1994\)007%3C1883:soacom%3E2.0.co;2](http://dx.doi.org/10.1175/1520-0442(1994)007%3C1883:soacom%3E2.0.co;2), <GotoISI>://WOS:A1994QC22600006, 1994.
- 625 Mlawer, E. J., Taubman, S. J., Brown, P. D., Iacono, M. J., and Clough, S. A.: Radiative transfer for inhomogeneous atmospheres: RRTM, a validated correlated-k model for the longwave, *Journal of Geophysical Research-Atmospheres*, 102, 16 663–16 682, doi:<http://dx.doi.org/10.1029/97jd002371>, <GotoISI>://WOS:A1997XN38400019, 1997.
- 630 Moorthi, S., Pan, H.-L., and Caplan, P.: Changes to the 2001 NCEP operational MRF/AVN global analysis/forecast system, *NWS Tech. Procedures Bulletin*, 484, <http://www.nws.noaa.gov/om/tpb/484.htm>, 2001.

Neggers, R. A. J., Koehler, M., and Beljaars, A. C. M.: A Dual Mass Flux Framework for Boundary Layer Convection. Part I: Transport, *Journal of the Atmospheric Sciences*, 66, 1465–1487, doi:<http://dx.doi.org/10.1175/2008jas2635.1>, (GotoISI)://WOS:000267263300001, 635 2009.

Pan, H. and Wu, W.: Implementing a mass flux convective parameterization package for the NMC Medium-Range Forecast model, NMC Office Note, 409, <http://www.emc.ncep.noaa.gov/officenotes/FullTOC.html#1990>, 1995.

Randall, D., Krueger, S., Bretherton, C., Curry, J., Duynkerke, P., Moncrieff, M., Ryan, B., Starr, D., Miller, M., 640 Rossow, W., Tselioudis, G., and Wielicki, B.: Confronting models with data - The GEWEX cloud systems study, *Bulletin of the American Meteorological Society*, 84, 455–469, doi:<http://dx.doi.org/10.1175/bams-84-4-455>, (GotoISI)://WOS:000182420400013, 2003.

Saha, S., Nadiga, S., Thiaw, C., Wang, J., Wang, W., Zhang, Q., Van den Dool, H. M., Pan, H. L., Moorthi, S., Behringer, D., Stokes, D., Pena, M., Lord, S., White, G., Ebisuzaki, W., 645 Peng, P., and Xie, P.: The NCEP Climate Forecast System, *Journal of Climate*, 19, 3483–3517, doi:<http://dx.doi.org/10.1175/jcli3812.1>, (GotoISI)://WOS:000239943100002, 2006.

Saha, S., Moorthi, S., Pan, H.-L., Wu, X., Wang, J., Nadiga, S., Tripp, P., Kistler, R., Woollen, J., Behringer, D., Liu, H., Stokes, D., Grumbine, R., Gayno, G., Wang, J., Hou, Y.-T., Chuang, H.-Y., Juang, H.-M. H., Sela, J., Iredell, M., Treadon, R., Kleist, D., Van Delst, P., Keyser, D., Derber, J., Ek, M., 650 Meng, J., Wei, H., Yang, R., Lord, S., Van den Dool, H., Kumar, A., Wang, W., Long, C., Chelliah, M., Xue, Y., Huang, B., Schemm, J.-K., Ebisuzaki, W., Lin, R., Xie, P., Chen, M., Zhou, S., Higgins, W., Zou, C.-Z., Liu, Q., Chen, Y., Han, Y., Cucurull, L., Reynolds, R. W., Rutledge, G., and Goldberg, M.: The NCEP climate forecast system reanalysis, *Bulletin of the American Meteorological Society*, 91, 1015–1057, doi:<http://dx.doi.org/10.1175/2010bams3001.1>, (GotoISI): 655 //WOS:000281704700004, 2010.

Sela, J.: Implementation of the sigma pressure hybrid coordinate into GFS., Tech. rep., NCEP office Note, 2009.

Siebesma, A. P. and Cuijpers, J. W. M.: Evaluation of parametric assumptions for shallow cumulus convection, *Journal of the Atmospheric Sciences*, 52, 650–666, doi:[http://dx.doi.org/10.1175/1520-0469\(1995\)052%3C0650:eopafs%3E2.0.co;2](http://dx.doi.org/10.1175/1520-0469(1995)052%3C0650:eopafs%3E2.0.co;2), 660 0469(1995)052<0650:eopafs>2.0.co;2, (GotoISI)://WOS:A1995QP83400002, 1995.

Siebesma, A. P., Bretherton, C. S., Brown, A., Chlond, A., Cuxart, J., Duynkerke, P. G., Jiang, H. L., Khairoutdinov, M., Lewellen, D., Moeng, C. H., Sanchez, E., Stevens, B., and Stevens, D. E.: A large eddy simulation intercomparison study of shallow cumulus convection, *Journal of the Atmospheric Sciences*, 60, 665 1201–1219, doi:[http://dx.doi.org/10.1175/1520-0469\(2003\)60%3C1201:alesis%3E2.0.co;2](http://dx.doi.org/10.1175/1520-0469(2003)60%3C1201:alesis%3E2.0.co;2), 0469(2003)60<1201:alesis>2.0.co;2, (GotoISI)://WOS:000182569200001, 2003.

Stevens, B., Lenschow, D. H., Vali, G., Gerber, H., Bandy, A., Blomquist, B., Brenguier, J. L., Bretherton, C. S., Burnet, F., Campos, T., Chai, S., Faloona, I., Friesen, D., Haimov, S., Laursen, K., Lilly, D. K., Loehrer, S. M., Malinowski, S. P., Morley, B., Petters, M. D., Rogers, D. C., Russell, L., Savic-Jovac, V., 670 Snider, J. R., Straub, D., Szumowski, M. J., Takagi, H., Thornton, D. C., Tschudi, M., Twohy, C., Wetzell, M., and van Zanten, M. C.: Dynamics and chemistry of marine stratocumulus - DYCOMS-II, *Bulletin of the*

- American Meteorological Society, 84, 579–+, doi:http://dx.doi.org/10.1175/bams-84-5.57910.1175/bams-84-5.579, <GotoISI>://WOS:000183223200017, 2003.
- 675 Stevens, B., Moeng, C. H., Ackerman, A. S., Bretherton, C. S., Chlond, A., De Roode, S., Edwards, J., Golaz, J. C., Jiang, H. L., Khairoutdinov, M., Kirkpatrick, M. P., Lewellen, D. C., Lock, A., Muller, F., Stevens, D. E., Whelan, E., and Zhu, P.: Evaluation of large-Eddy simulations via observations of nocturnal marine stratocumulus, *Monthly Weather Review*, 133, 1443–1462, doi:http://dx.doi.org/10.1175/mwr2930.110.1175/mwr2930.1, <GotoISI>://WOS:000230028000003, 2005.
- 680 Sundqvist, H.: Parameterization scheme for non-convective condensation including prediction of cloud water content, *Quarterly Journal of the Royal Meteorological Society*, 104, 677–690, doi:http://dx.doi.org/10.1002/qj.4971044411010.1002/qj.49710444110, <GotoISI>://WOS:A1978FJ77400009, 1978.
- Troen, I. and Mahrt, L.: A simple model of the atmospheric boundary layer - sensitivity to surface evaporation, *Boundary-Layer Meteorology*, 37, 129–148, doi:http://dx.doi.org/10.1007/bf0012276010.1007/bf00122760, <GotoISI>://WOS:A1986E265800008, 1986.
- 685 Xiao, H., Mechoso, C. R., Sun, R., Han, J., Park, S., Hannay, S., Teixeira, J., and Bretherton, C.: Diagnosis of Marine Low Clouds Simulation in the NCAR Community Earth System Model (CESM) and the NCEP Global Forecast System (GFS)-Modular Ocean Model v4 (MOM4) coupled model, *Climate Dynamics*, 43, 737–752, 2014.
- 690 Xu, K. M. and Randall, D. A.: A semiempirical cloudiness parameterization for use in climate models, *Journal of the Atmospheric Sciences*, 53, 3084–3102, doi:http://dx.doi.org/10.1175/1520-0469(1996)053<3084:ascpfu>2.0.co;2, <GotoISI>://WOS:A1996VT96600006, 1996.
- 695 Zhao, Q. Y. and Carr, F. H.: A prognostic cloud scheme for operational NWP models, *Monthly Weather Review*, 125, 1931–1953, doi:http://dx.doi.org/10.1175/1520-0493(1997)125<1931:apcsfo>2.0.co;2, <GotoISI>://WOS:A1997XP30300014, 1997.
- 700 Zhu, P., Bretherton, C. S., Kohler, M., Cheng, A. N., Chlond, A., Geng, Q. Z., Austin, P., Golaz, J. C., Lenderink, G., Lock, A., and Stevens, B.: Intercomparison and interpretation of single-column model simulations of a nocturnal stratocumulus-topped marine boundary layer, *Monthly Weather Review*, 133, 2741–2758, doi:http://dx.doi.org/10.1175/mwr2997.110.1175/mwr2997.1, <GotoISI>://WOS:000231952300014, 2005.

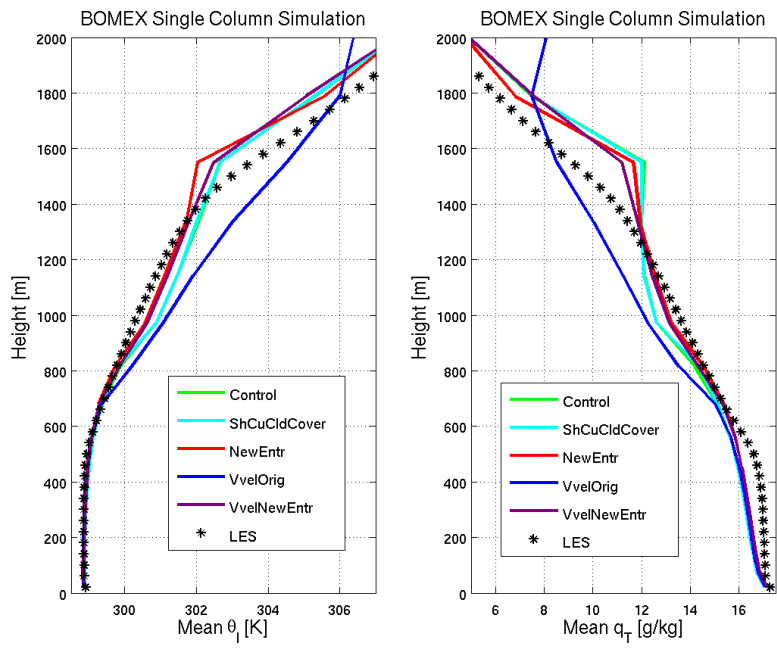


Fig. 1. BOMEX liquid water potential temperature (left) and total water (right) profiles averaged over hours 3-6. Coloured lines are different SCM experiments; black stars are LES.

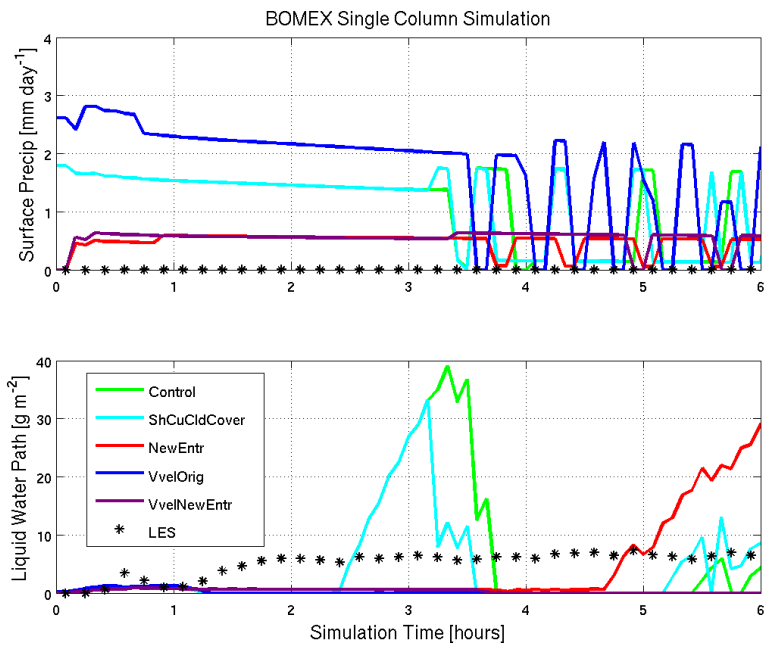


Fig. 2. BOMEX time series of surface precipitation rate (top) and liquid water path (bottom) in the first six hours of simulation. Coloured lines are different SCM experiments; black stars are LES.

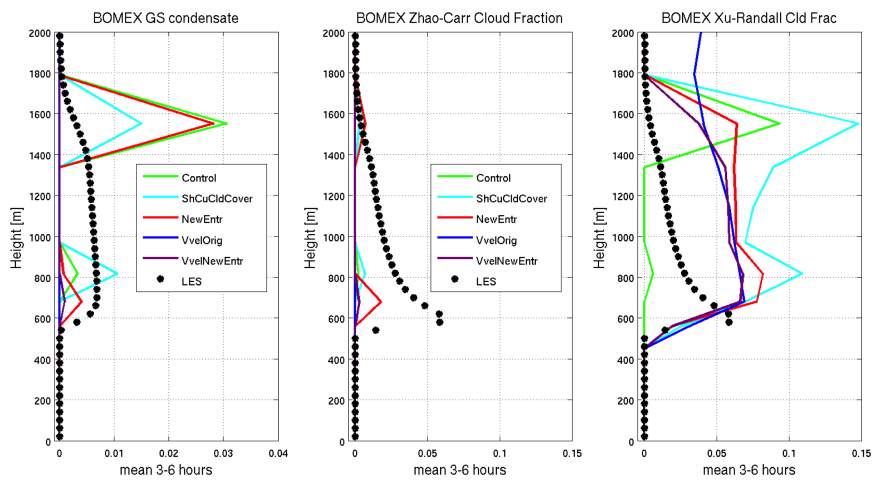


Fig. 3. BOMEX grid scale condensate (left, g/kg) and cloud fraction as calculated in the stratiform microphysics (centre) and radiation (right) parametrisations, averaged over hours 3-6. Coloured lines are different SCM experiments; black stars are LES.

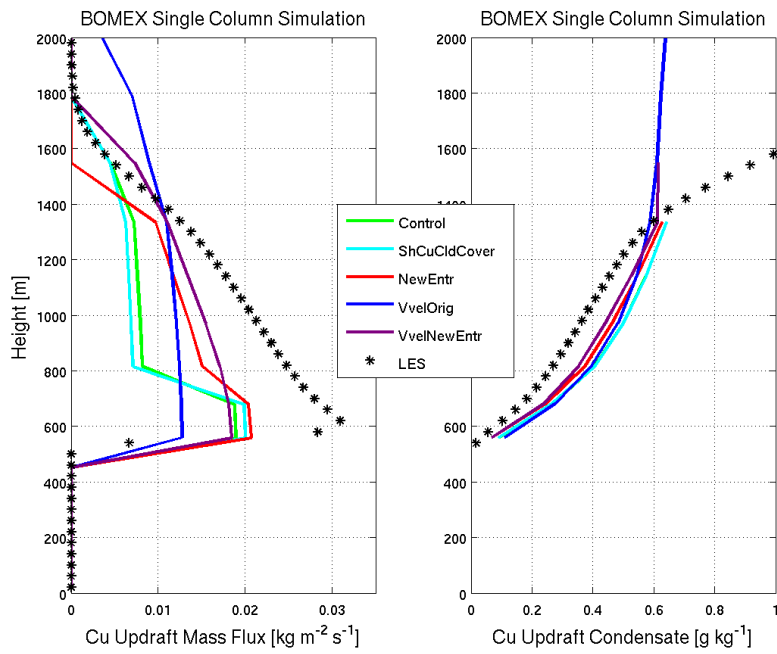


Fig. 4. BOMEX shallow cumulus updraught (left) mass flux and (right) condensate profiles averaged over hours 3-6. Coloured lines are different SCM experiments; black stars are LES.

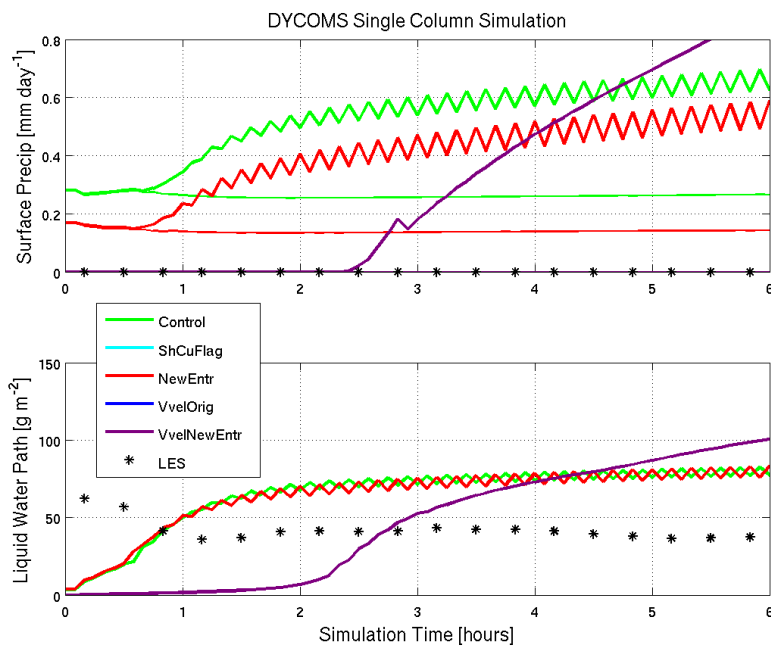


Fig. 5. DYCOMS time series of surface precipitation rate (top) and liquid water path (bottom) in the first six hours of simulation. Coloured lines are different SCM experiments; black stars are LES. Results are identical for all experiments without shallow convection, thus ShCuFlag and VvelOrig are hidden by VvelNewEntr.

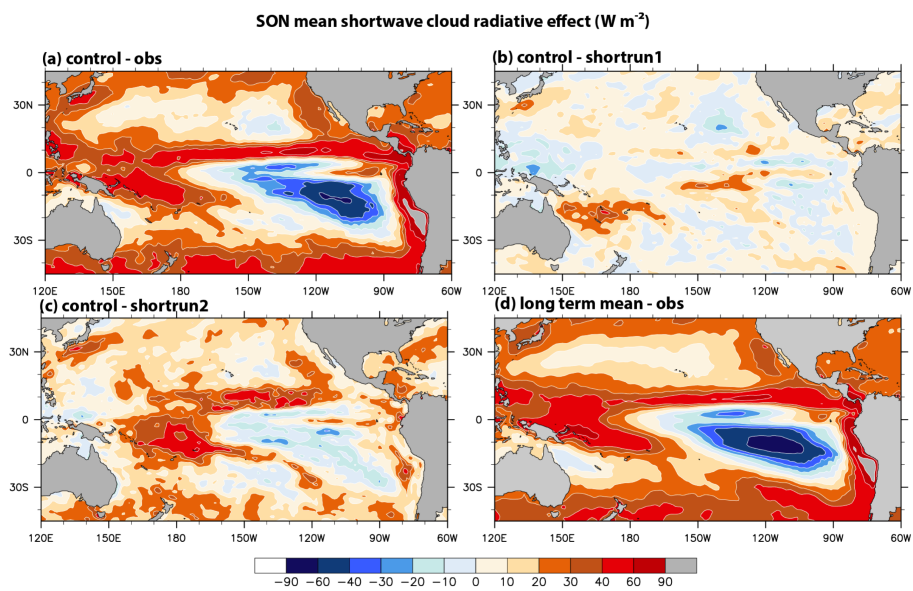


Fig. 6. Shortwave cloud forcing biases and their improvements in global simulations. Panel a) shows the bias in the control run compared to observations; panel b) shows the difference between control and shortrun1; panel c) shows the difference between control and shortrun2. In panels b) and c), the respective experiment bias has been eliminated to the extent that the pattern matches a). See text for further explanation. Panel d) shows the bias in the 50 year control run.

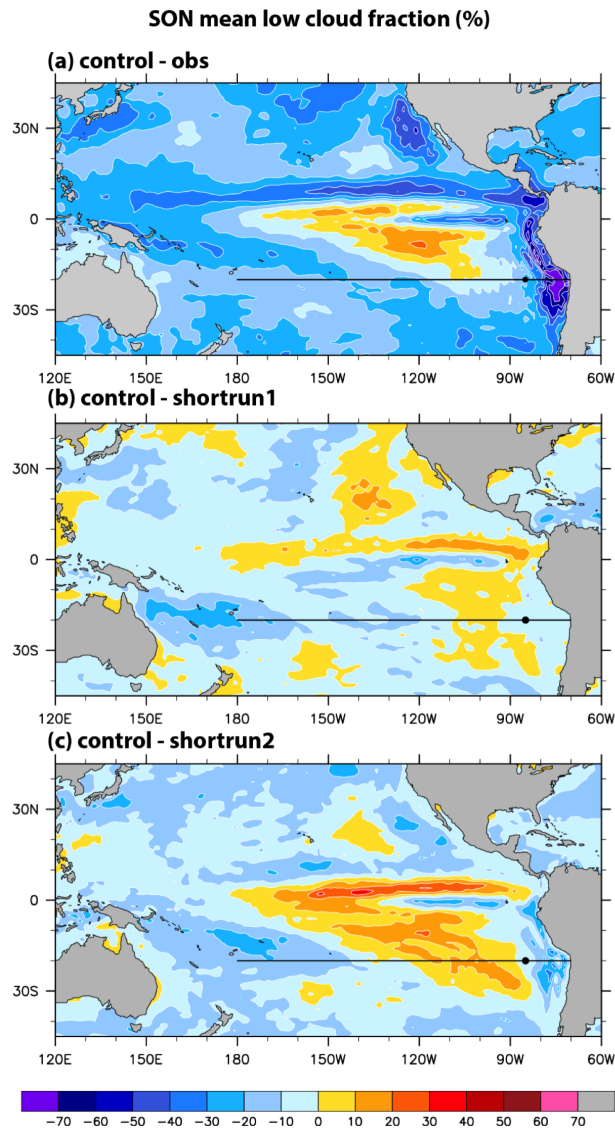


Fig. 7. Cloud fraction bias and its improvement in global simulations. Panel a) shows the bias in the control run compared to observations; panel b) shows the difference between control and shortrun1; panel c) shows the difference between control and shortrun2. In panels b) and c), the respective experiment bias has been eliminated to the extent that the pattern matches a). See text for further explanation.

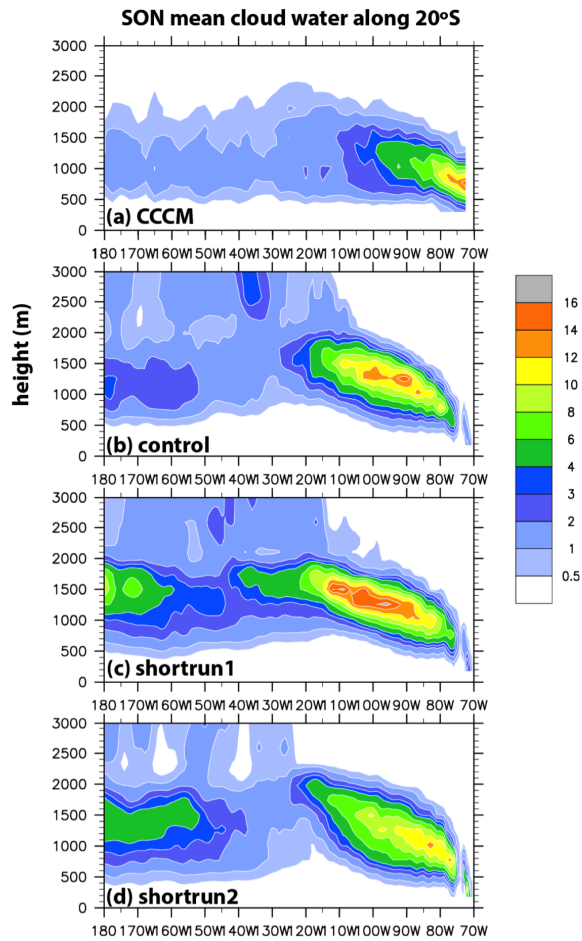


Fig. 8. Cloud condensate along the 20 S Pacific cross section in a) observations; b) the control run; c) shortrun1, and d) shortrun2.

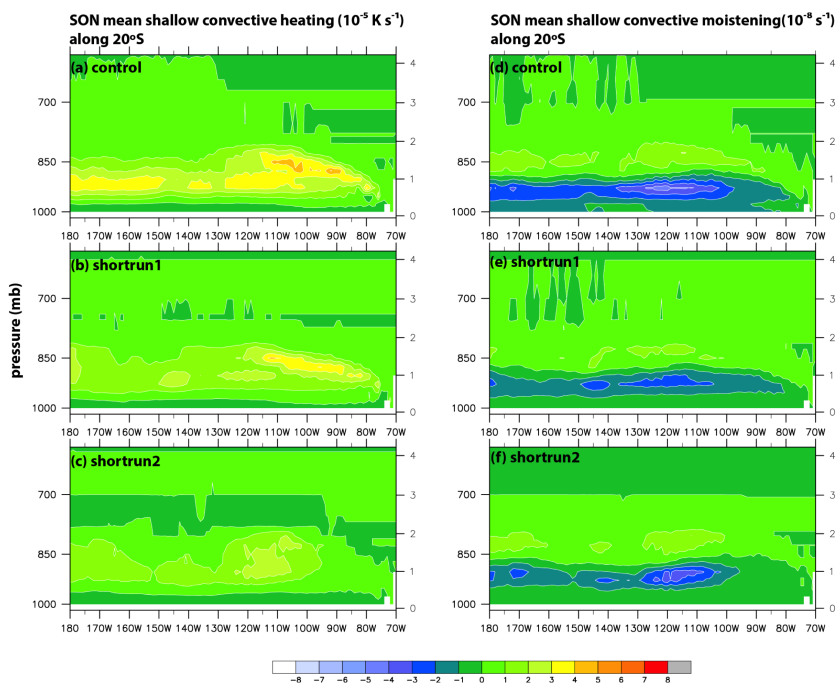


Fig. 9. Shallow cumulus heating (left column) and moistening (right column) in the control run (top), shortrun1 (middle), and shortrun2 (bottom).

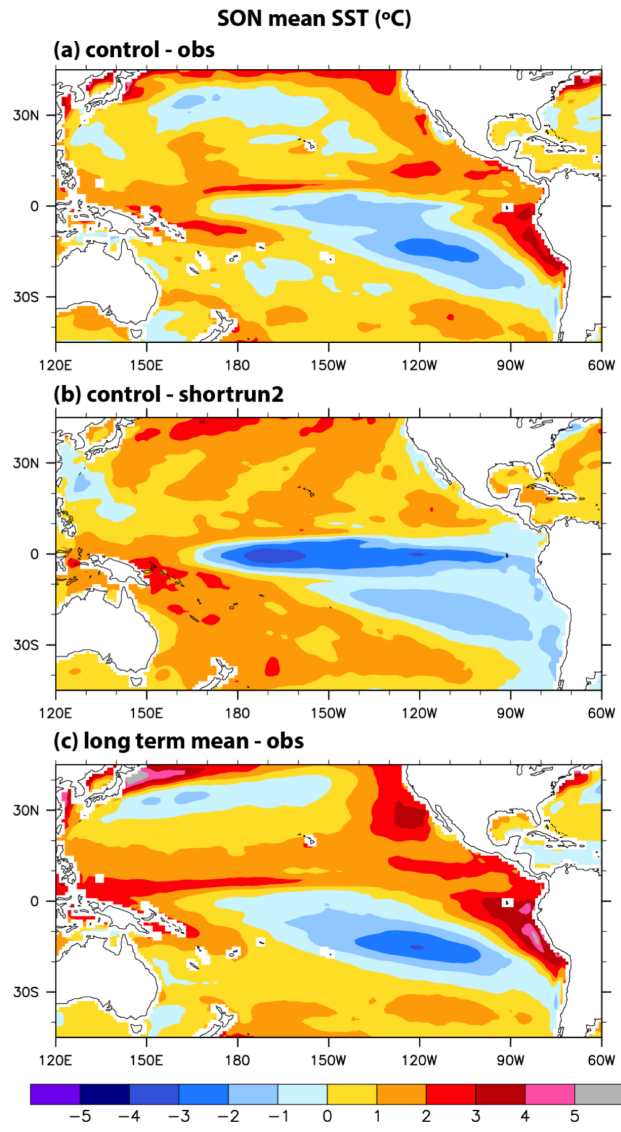


Fig. 10. Pacific SST in global simulations: a) bias in the control run; b) the difference between control and shortrun2, and c) bias in the 50 year control run. In panel b), the experiment has eliminated the bias to the extent that the pattern matches that of panel a). See text for further explanation.

Table 1. Parameter settings for SCM experiments with the BOMEX shallow convection cases. Parameters a and b refer to coefficients in eqn. 4

	<i>Control</i>	<i>ShCuCldCover</i>	<i>NewEntr</i>	<i>VvelOrig</i>	<i>VvelNewEntr</i>
ShCu cloud	No	Yes	Yes	Yes	Yes
c	0.3	0.3	1.0	0.3	1.0
c_0 [m^{-1}]	2.0×10^{-3}	2.0×10^{-3}	1.0×10^{-3}	2.0×10^{-3}	1.0×10^{-3}
c_1 [m^{-1}]	5.0×10^{-4}	5.0×10^{-4}	2.5×10^{-4}	5.0×10^{-4}	2.5×10^{-4}
a	NA	NA	NA	$\approx \frac{1}{3}$	$\approx \frac{1}{3}$
b	NA	NA	NA	≈ 6	≈ 6

Table 2. Parameter settings for free-running coupled global model experiments.

	<i>Control</i>	<i>Shortrun1</i>	<i>Shortrun2</i>
ShCu Cloud	No	No	Yes
c	0.3	1.0	1.0
c_0 [m^{-1}]	2.0×10^{-3}	1.0×10^{-3}	1.0×10^{-3}
c_1 [m^{-1}]	5.0×10^{-4}	5.0×10^{-4}	2.5×10^{-4}
a	NA	NA	$\approx \frac{1}{3}$
b	NA	NA	≈ 6
ShCu Depth Flag	No	No	Yes
PBL Bckgrnd Diff [m^2/s]	0.3	0.3	0.1
TKE Dissipative Heating	No	No	Yes